Effect of Geometric Size on Static Strength Properties of Porous Alumina

NATSUMI MIYAZAKI, TOSHIHIKO HOSHIDE, DAICHI ITAYA
Department of Energy Conversion Science
Kyoto University Graduate School of Energy Science
Yoshida-Honmachi, Sakyo-ku, Kyoto 606-8501
JAPAN
miyazaki.natsumi.35z@st.kyoto-u.ac.jp

Abstract: - In applications of porous ceramics to elements in energy related components, their strength properties should be appropriately evaluated to guarantee in-service durability. In this work, bending strength properties of porous alumina specimens with four different shapes were investigated to clarify geometrical size effects depending on porosity. 3-point bending tests were conducted using notched specimens as well as smooth specimens of three distinct sizes. It was revealed that the bending strength decreased drastically as increasing porosity. An effective volume concept was introduced in discussing geometric size effect. Average strength was correlated with effective volume for specimens with respective porosities. A little bit of dispersion was seen, though the average strength for all materials was well correlated with the effective volume independently of specimen geometry. Cross-sections were observed through a laser scanning microscope to characterize spatial and size distributions of pores. In this study, based on the observed pore characteristics, a fracture mechanics procedure was proposed by presuming pores to be surrounded by virtual cracks. Monte Carlo simulations based on the proposed procedure were carried out by assuming the same characteristics of crack distribution as those of pore distribution in a material. Strength simulated by using the proposed procedure almost coincided with experimentally observed one. Consequently, the proposed procedure was confirmed to be applicable to evaluation of porosity and geometric size effects on strength.

Key-Words: - alumina, porosity, bending strength, size effect, effective volume, fracture mechanics.

1 Introduction

It is well known that porous ceramics have higher heat-resistance and larger specific surface area compared with dense ceramics. Therefore, applications of porous ceramics are expected in energy related elements, e.g. filter, catalyst, and so on. Since porous ceramics are practically used with specified shapes and sizes, strength properties should be adequately evaluated for porous ceramics with various geometries.

Strength properties are often obtained by using specimens with standard geometries. It has been reported, however, that specimen geometry as well as loading mode affects strength characteristics in dense ceramics [1-12]. In addition, for successful application of porous ceramics to engineering components, strength characteristics of notched components should be also investigated in the relation to the well-known size effect. For such an analysis, an effective volume proposed by Davis [13] was successfully used to evaluate effects of specimen geometry and/or loading mode on average strength [14]. It is not clarified, however, that the effective volume can be applied to strength evaluations in porous ceramics.

In this work, commercial alumina ceramics having different porosities were selected, and bending tests were conducted using specimens with four different geometries. Effects of specimen geometry on strength was clarified experimentally. Since strength of porous ceramics may be affected by spatial and size distributions of pores as well as bulk porosity, pore-characteristics were also determined quantitatively based on observations of cross-sections through a laser scanning microscope. A fracture mechanics procedure, which was proposed in a previous work [15], was developed to evaluation of geometry effect on strength by using the determined pore-characteristics. The applicability of the effective volume to the size effect on strength in porous ceramics was also discussed based on results simulated by using the developed procedure.

2 Experimental Procedures

2.1 Materials

Commercial alumina ceramics are applied for

investigating geometry effects of specimens having different porosities on strength. This work was conducted by using two porous alumina ceramics with porosities p = 34.9% and 48.4% as well as a dense alumina with a porosity of 0.803%. In the following, the three materials with p = 0.803%, 34.9%, and 48.4% are respectively designated as AL-01, AL-35, and AL-48, according to their percentage values of porosity.

Table 1. Physical properties of alumina ceramics.

Material	AL-01	AL-35	AL-48
Porosity p (%)	0.803	34.9	48.4
Bulk density (Mg/m^3)	3.95	2.59	2.05
Water absorption (%)	0.00	13.9	30.0
Purity (%)	99.7	99.5~	97.0~
Vickers hardness (HV)	2030	179	15.7
Theoretically estimated fracture toughness K_{Cp} (MPa·m$^{1/2}$)	3.33	0.797	0.065

Physical properties of the three materials are summarized in Table 1. Vickers hardness was measured under indentation force of 9.807N and holding time of 15s. Values of fracture toughness K_{Cp} in the table have been estimated in a previous work [15].

2.2 Specimen preparations

Smooth specimens of three types and notched specimen were prepared for the respective materials of AL-01, AL-35 and AL-48. Shapes and dimensions of specimens to be examined are shown in Fig. 1. The specimen as shown in Fig. 1(a) is the same as the standard bending specimen specified in JIS R 1601 [16]. As shown in Fig. 1(d), notched specimens were prepared by machining semicircular notches on the smooth specimens as shown in Fig. 1(b), and the semicircular notched has a root radius of 3mm. In the following, the three smooth specimens as shown in Figs. 1(a), 1(b) and 1(c) will be respectively designated JIS-SD, JIS-H2 and JIS-DB, and the notched specimen will be designated NTS-R3.

Twenty specimens were applied to bending strength tests for respective specimens of JIS-SD, JIS-H2, JIS-DB and NTS-R3. Consequently, twenty strength data were obtained for each specimen type.

2.3 Bending test

All bending tests were conducted under three-point bending mode with a span length of 20mm in an ambient atmosphere, i.e. 294±5K and 40±14% relative humidity. Bending tests were conducted by using a closed-loop hydraulic testing machine, and the loading rate was controlled so that the rate of the maximum tensile stress generated in a specimen might be about 100MPa/s. The bending strength of a specimen was evaluated as the maximum stress monitored at its fracture.

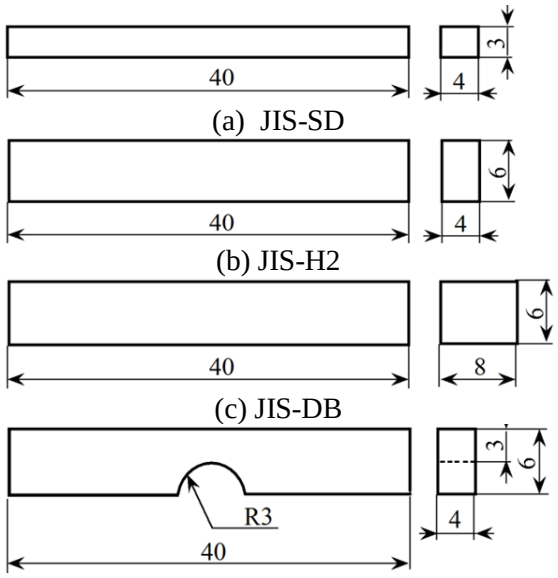

Fig. 1 Specimen shape.

3 Experimental Results and Discussion

3.1 Bending strength

It is well known that large scatters are observed in strength properties of brittle materials, especially ceramics to be investigated in this work. In this work, too, bending strength σ_f is analyzed statistically, and its distribution is expressed by using Weibull distribution function. The cumulative probability function $F(\sigma_f)$ of bending strength σ_f is expressed as (1) by using three-parameter Weibull model [17].

$$F(\sigma_f) = 1 - \exp\left[-\left(\frac{\sigma_f - \sigma_L}{\sigma_S}\right)^m\right] \qquad (1)$$

In (1), σ_L, σ_S and m are respectively location parameter, scale parameter and shape parameter.

Table 2. Statistical parameters of bending strength.

Material	Specimen shape	Average strength $\sigma_{f,ave}$ (MPa)	Coefficient of variation *COV*	Parameters in two-parameter Weibull distribution		Parameters in three-parameter Weibull distribution		
				Scale param. σ_S (MPa)	Shape param. *m*	Scale param. σ_S (MPa)	Shape param. *m*	Location param. σ_L (MPa)
AL-01	JIS-SD	569	0.0462	580	25.4	72.5	2.36	505
	JIS-H2	470	0.0896	488	13.3	133	3.02	351
	JIS-DB	427	0.144	454	7.44	-	-	-
	NTS-R3	468	0.0642	481	18.4	86.8	2.45	391
AL-35	JIS-SD	69.0	0.0426	70.4	27.6	12.7	4.23	57.5
	JIS-H2	60.1	0.145	63.5	8.32	19.6	1.82	43.0
	JIS-DB	70.0	0.0940	72.9	12.2	20.1	2.65	52.2
	NTS-R3	83.8	0.111	87.8	10.3	30.4	2.90	56.8
AL-48	JIS-SD	5.91	0.0732	6.08	16.3	1.07	2.20	4.95
	JIS-H2	7.19	0.144	7.60	8.36	2.09	1.62	5.35
	JIS-DB	11.5	0.115	12.1	9.90	5.19	3.69	6.81
	NTS-R3	10.7	0.141	11.3	8.64	4.05	2.51	7.13

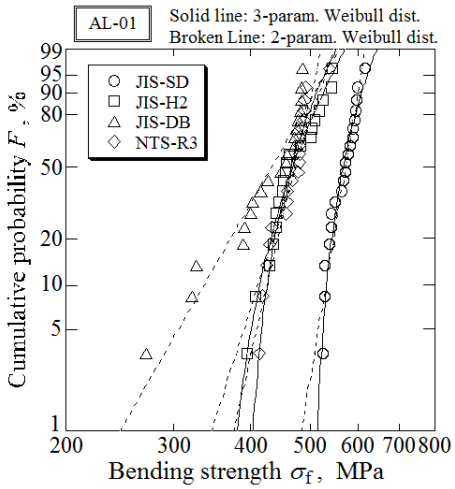

Fig. 2 Weibull plot of strength in AL-01.

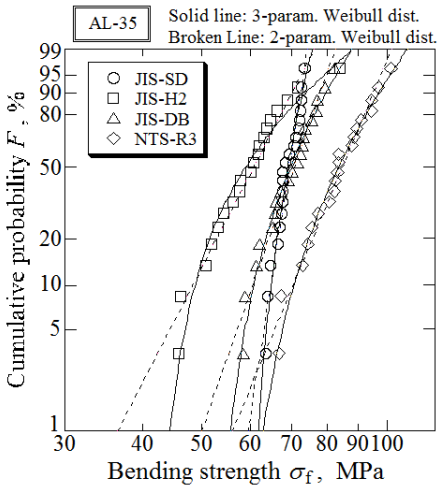

Fig. 3 Weibull plot of strength in AL-35.

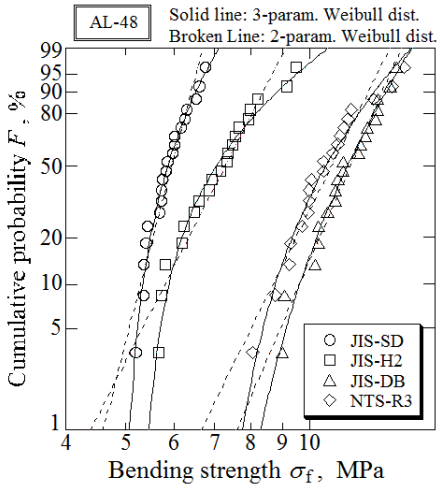

Fig. 4 Weibull plot of strength in AL-48.

The statistics of bending strength are summarized in Table 2. As seen in Table 2, it appears that the coefficient of variation is smaller and the shape parameter is larger in JIS-SD type specimen compared with those in JIS-H2, JIS-DB and NTS-R3 type specimens. This implies that a relative scatter of strength is smallest in JIS-SD type specimen.

Figures 2~4 present distributions of strength σ_f, which are plotted on Weibull probability paper. The curved lines in Figs. 2~4 represent $F(\sigma_f)$, fitted to (1). The broken straight lines in Figs. 2~4 show lines fitted to two-parameter function, which is given by setting $\sigma_L = 0$ in (1). As seen in Fig. 2, the strength distribution of AL-01 shifts toward higher strength region in order of JIS-DB, NTS-R3, JIS-H2, JIS-SD. On the other hand, as seen in Figs. 3 and 4, the strength distributions in AL-35 and AL-48 materials shift toward higher strength region in order of JIS-H2, JIS-SD, JIS-DB, NTS-R3 and JIS-SD, JIS-H2, NTS-R3, JIS-DB, respectively.

3.2 Effective volume and its correlation to bending strength

The effective volume has been applied to explain the strength characteristics depending on the specimen geometry and/or the loading mode [14]. Davis [15] derived the effective volume from the two-parameter Weibull model [17] for a homogeneous material with a volume V. In a material subjected to an arbitrary stress state σ_v in infinitesimal small volume element dv, the effective volume V_E is defined as a volume integration: i.e.

$$V_E = \int_V \left(\frac{\sigma_v}{\sigma_R} \right)^m dv \tag{2}$$

In (2), σ_R is a representative stress and m is the shape parameter in the two-parameter Weibull distribution function. The maximum nominal stress generated in a component is usually adopted as σ_R and is also used as its fracture strength. It is noteworthy that (2) is implicitly based on some basic assumptions as follows. The shape parameter and the flaw population must be independent of specimen geometry and/or loading mode for the same material. Another presumption is associated with flaw size and density in a small volume dv in the volume integration: the number of flaws must not be constant or there may be no flaws in such a small volume element with reducing dv infinitesimally small. In this work, however, the aforementioned assumptions are supposed to be extendable to finite volumes in dense and porous ceramics in the following application of effective volume concept.

Fracture of a component occurs in its region, which consists of infinitesimally small volume with positive σ_v. Therefore, a volume integration of (2) should be executed in the restricted region. The effective volume is calculated to correlate the bending strength in experiment as follows. For smooth specimen under three-point bending with a double outer span to inner span ratio as in the present experiment, the effective volume is theoretically calculated from (2) as:

$$V_E = \frac{V}{2(m+1)^2} \tag{3}$$

In (3), V is the whole volume in a region within an outside span of a smooth specimen. On the other hand, the effective volume for a notched specimen is evaluated using stress distribution given by a finite element analysis, as in the next equation:

$$V_E = \sum_i \left(\frac{\sigma_i}{\sigma_{max}} \right)^m V_i \tag{4}$$

In (4), σ_i and σ_{max} are the normal stress in the i-th element in the mesh of notched specimen and the maximum stress calculated by the finite element analysis, respectively. The volume of the i-th element, V_i, is given by multiplying the area of the element by its thickness. The summation with respect to i in (4) is made only for elements where the normal stress in the longitudinal direction of a specimen is positive for the same reason as in the volume integration. Although a direct verification on the validity of the evaluation using (4) cannot be made for the notched specimens due to lack of theoretical stress distribution, the validity is verified for smooth specimens by confirming the difference within ±5% between the theoretical calculation by (3) and the result evaluated by (4). The calculated values of effective volume are listed in Table 3.

Table 3. Effective volume of alumina specimens with different shapes (in mm^3).

	JIS-SD	JIS-HD	JIS-DB	NTS-R3
AL-01	0.4473	0.8945	1.789	0.1998
AL-35	0.4138	0.8275	1.655	0.1914
AL-48	0.7643	1.529	3.057	0.2761

In Fig. 5, the mean strength $\sigma_{f,m}$ for each type of

specimen is correlated with the effective volume V_E evaluated by using (3) and (4) for the corresponding specimen type. The m value for each type of specimen, which was obtained by fitting to two-parameter Weibull distribution function, was different each other mentioned previously. So, values of m were averaged, and the averaged m value was adopted in calculating V_E. The mean values of strength for components with the effective volumes of V_{E1} and V_{E2} are expressed as $\sigma_{f,m1}$ and $\sigma_{f,m2}$, respectively. Then, the following relationship is given [13]:

$$\frac{\sigma_{f,m1}}{\sigma_{f,m2}} = \left(\frac{V_{E1}}{V_{E2}} \right)^{-1/m} \tag{5}$$

When the mean strength $\sigma_{f,ref}$ corresponding to a reference effective volume $V_{E,ref}$ is given, the relation between an arbitrary effective volume V_E and its corresponding mean strength $\sigma_{f,m}$ is expressed from Eq. (5) as follows.

$$\sigma_{f,m} = \sigma_{f,ref} \, (V_{E,ref})^{1/m} \, (V_E)^{-1/m} \tag{6}$$

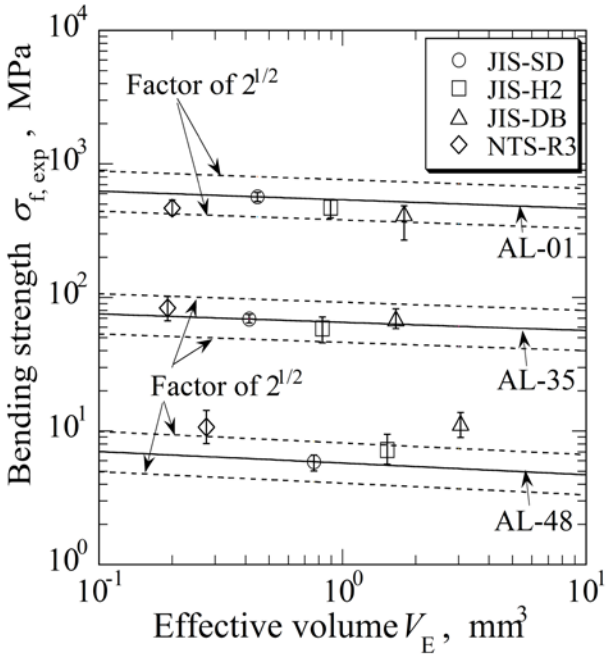

Fig. 5 Correlation of mean strength in experiments with effective volume.

This implies that the relation between $\sigma_{f,m}$ and V_E can be expressed with a straight line when values of these parameters are plotted on log-log diagram.

The straight lines in Fig. 5 present the relations of (6) passing the data points corresponding to the result in JIS-SD type specimen. The dotted lines present a scatter band corresponding to factor of $2^{1/2}$. In AL-01, the mean strength is found to be correlated with the effective volume independently of specimen geometry. The reason why the mean strength in NTS-R3 is lower than others is associated with grinding-induced flaws generated on the notch root, which are perpendicular to normal stress. On the other hand, in AL-35 and AL-48, these results also show a similar tendency, although these do not necessarily correspond to (6). Because (6) is originally derived for dense material, it is suggested that the relation (6) cannot be applied directly for porous materials.

3.3 Fractography

Fracture surfaces of alumina ceramics were observed by a scanning electron microscope (SEM). Examples of SEM photographs of fracture surfaces are shown in Figs. 6 and 7. Figure 6(a) presents a typical morphology in fracture surface with fracture origin from an inherent flaw in the dense AL-01 material. On the other hand, in AL-35 and AL-48 materials, fracture surfaces seem rough and featureless, and the fracture origin cannot be identified, as seen in Figs. 6(b), 6(c) and Fig. 7. In these porous materials, clusters of pores were frequently observed. It has been reported that a similar morphology appears in porous ceramic materials [18].

Cross-sections were also observed through a laser scanning microscope (LSM) to characterize spatial and size distributions of pores. Figure 8 presents LSM photographs of cross-sections in porous materials. Pores in AL-48 are found to be larger compared with those in AL-35. By binary-digitizing LSM data, size distributions and densities of pores in AL-35 and AL-48 are quantified, and the data will be used in the following simulation.

(a) (b) (c)

Fig. 6 SEM photographs of overall fracture surfaces: (a) AL-01, (b) AL-35 and (c) AL-48.

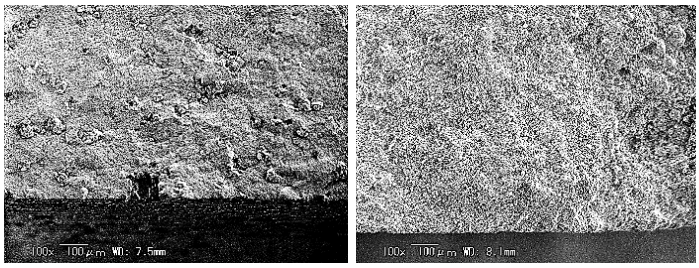

(a) (b)

Fig. 7 SEM photographs of fracture surfaces in porous materials observed with higher magnification: (a) AL-35 and (b) AL-48.

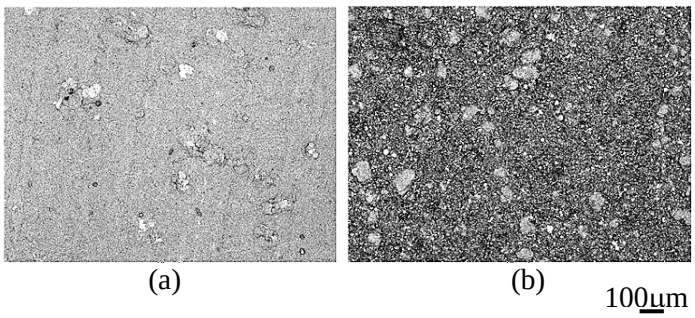

(a) (b)

Fig. 8 LSM photographs of specimen surfaces on porous ceramics: (a) AL-35 and (b) AL-48.

4 Numerical Simulation of Strength Affected by Pores

4.1 Modeling of flaws/pores

Inherent flaws generated during a sintering process are distributed in a specimen. In this simulation, a fracture mechanics procedure was proposed by presuming pores to be surrounded by virtual cracks.

In the simulation, such flaws/pores are modeled as circular, semi-elliptic or quarter-elliptic cracks. Cracks in a specimen are randomly located only within the region, which is subjected to tensile stress in the specimen. It is assumed that the failure of specimen occurs when the maximum values among all intensity factors, K_{max}, is just equal to the fracture toughness K_C of a material under consideration. Such a calculation is repeated to reach a specified number of specimens.

In determining positions of individual cracks, a Cartesian *x*-*y*-*z* coordinate is introduced within the tensile region of a specimen. In this coordinate, *x*- and *y*-axes are respectively parallel and vertical to the longitudinal direction of the specimen and *z*-axis is the transverse direction (width direction) of a specimen (see Fig. 9). By considering no stress gradient in the width direction (*z*-axis) of specimen under bending mode, positions of cracks existing in an arbitrary cross-section are projected in the *z* direction and onto the *x*-*y* plane. Therefore, in the simulation, the position (*x*, *y*) of a crack is prescribed on the *x*-*y* plane. For example, the position of *i*-th crack in a specimen is described as (x_i, y_i) on the *x*-*y* plane as shown in Fig. 9. Crack positions are randomly set by using a series of quasi-uniform random numbers generated by a computer. According to crack position, cracks are classified into three types, i.e., embedded, surface, and corner cracks, which are respectively illustrated in Fig. 10. The depth *h* of the center of an original circular crack is the distance from the specimen

surface. The length a and c are radius of an original circular crack and the depth of a modeled crack, respectively.

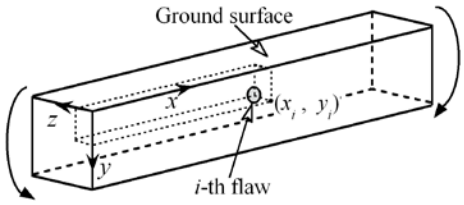

Fig. 9 Cartesian coordinate in specimen subjected to bending.

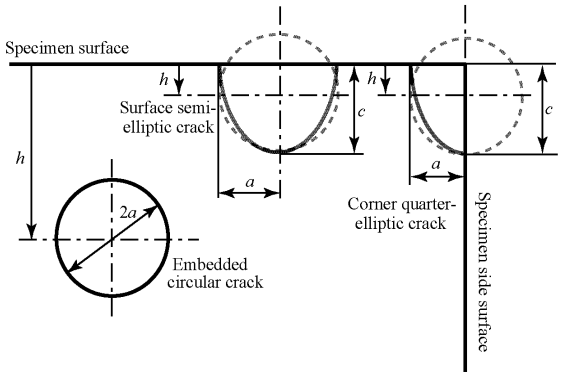

Fig.10 Schematic illustration of crack patterns.

The size a of each crack is given independently of its location by using a different series of quasi-uniform random numbers. The size distributions for inherent flaw generated during a sintering process expressed by using function $F(a)$ of cumulative probability as follows:

$$F(a) = 1 - \exp\left[-\left(\frac{a - a_{\mathrm{L}}}{a_{\mathrm{S}}}\right)^{\gamma}\right] \tag{7}$$

The above equation is of Weibull type consisting of three parameters.

4.2 Procedure and parameters in simulation

It has been reported [19-22] that a fracture-mechanics-based criterion for long cracks cannot be directly applied to the strength evaluation of ceramic components, which are fractured originating from small inherent cracks. In this simulation, the following approximation [20] is adopted in the evaluation of a valid K value for a small crack with length a:

$$K = \sigma_{\mathrm{a}} [\pi (a + l_0)]^{1/2} M_K \tag{8}$$

A length parameter l_0 is crack length to be added to the original crack length a. In (8), σ_{a} is the applied stress, and M_K is a magnification factor given by considering the shape and location of the crack as well as the stress distribution in a specimen. The value of M_K is determined using published numerical results [23-25] according to the aforementioned situations of crack. The maximum $K_{\max}$ is obtained among all K values calculated for cracks located in a specimen, and the applied stress σ_{a} at the fracture of the specimen is designated as the strength σ_{f}. The fracture criterion, i.e., $K_{\max} = K_{\mathrm{C}}$, combined with (8) is written as follows:

$$\sigma_{\mathrm{a}} = \frac{K_{\mathrm{C}}}{\sqrt{\pi (a + l_0) M_K}} \tag{9}$$

Using (9), the strength value of one specimen is finally determined by the length a and the magnification factor M_{K} of crack dominating a fracture of the specimen. Figure 11 shows the flow chart of the present simulation.

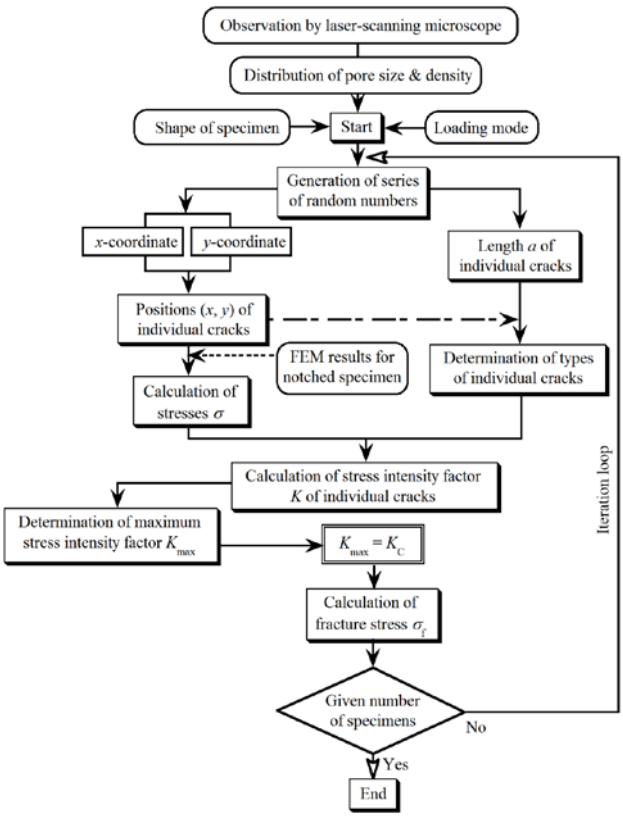

Fig. 11 Flow chart of simulation.

A grinding-induced residual stress exists usually in a ground specimen, and affects the strength properties. Such a residual stress, however, is generally known to be compressive on the ground surface. In a previous work, the strength of ground ceramics was simulated by considering a grinding-

induced residual stress, and it was elucidated that the strength increased up to about 40 MPa due to compressive residual stress. In general, however, it is not easy to measure/estimate a grinding-induced residual stress, and ignoring such an effect results in conservative estimation of strength. Consequently, for practical application, the effect of grinding-induced residual stress is not considered in the present simulation.

Parameters used in simulations are summarized in the following. Parameters, which have been used in a previous work [26], are applied in simulations for AL-01. Size distributions and densities of cracks in AL-35 and AL-48 are applied by using LSM data. The number of surface cracks is given by the crack density and relative crack positions on the specimen surface, though corner cracks and surface cracks are not classified in the analysis. Table 4 summarizes other numerical parameters, such as size distributions and densities of pores/cracks, which are applied to simulations. Values of fracture toughness for the three materials has been estimated appropriately by using average pore radius and average bending strength, based on fracture mechanics criterion [15].

Table 4. Characteristics of pores/crack-sizes and their distributions.

Material	AL-01	AL-35	AL-48
Density d_C (1/mm^3)	1.25	83.6	112
Shape parameter γ	7.7	1.3	0.97
Location parameter a_L (μm)	1.0	7.14	5.73
Scale parameter a_S (μm)	25	21.6	16.1
Maximum pore size a_{max} (μm)	25	150	180
Average pore size a_{ave} (μm)	0	29.0	24.9

The modification using (8) is applied in evaluation of a valid K value for a small flaw. The additional crack length l_0 in (8) is set to be 10 μm on the basis of the previous work for alumina ceramics [15].

In the following, a Monte Carlo simulation is carried out for the same shaped specimen under the same loading mode as those adopted in the experiment. In the present simulation, the loop calculation shown in Fig. 11 is iterated 100 times for the respective type of specimen. Actually, 100 trials are made by creating 100 different combinations of spatial and size distributions of cracks by using random numbers generated in a computer. Consequently, the aforementioned simulation gives 100 strength data for each type of the specimen.

4.3 Simulated result and discussion

Figure 12 shows comparison of simulated and experimental strength data. The broken line presents a scatter band corresponding to a factor of 2. Error bars in horizontal and vertical directions indicate scatter ranges in simulated and experimental results, respectively. By comparing the simulated results with the experimental ones, a good agreement between them is seen within the range of factor of 2, independently of specimen geometry and material.

In this work, it is assumed that pores are surrounded by virtual cracks. By the assumption, stress concentrations at tips of a pores and a crack become identical. Consequently, it may be concluded that strength properties and effect of geometric size on strength properties of porous alumina are well explained by the proposed procedure based on fracture mechanics. In other words, it is suggested that the proposed procedure is applicable to strength evaluation for porous ceramic materials.

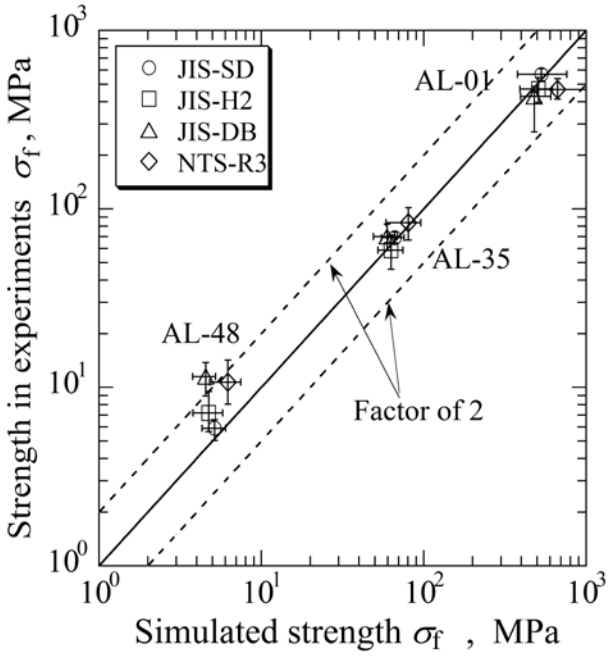

Fig. 12 Comparison of simulated and experimental strength.

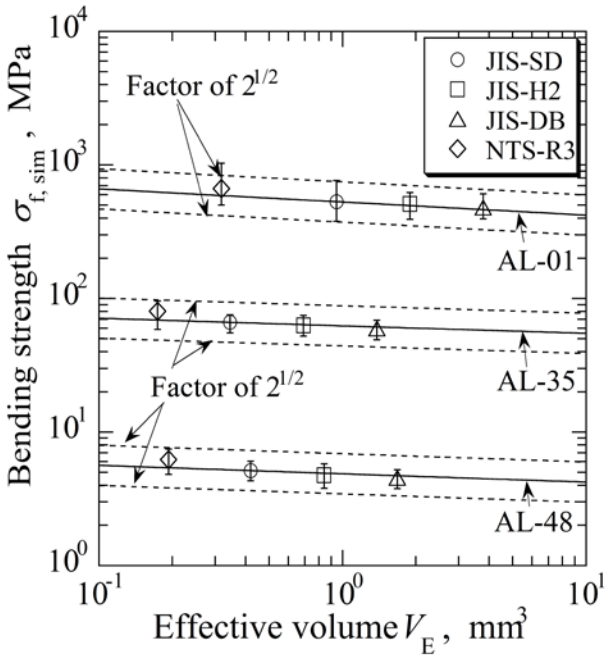

Fig. 13 Correlation of simulated strength with effective volume.

Figure 13 shows correlation of simulated strength with effective volume. By comparing the simulated results in Fig. 13 with the experimental ones in Fig. 5, the mean strength in NTS-R3 is fitted to the theoretical relation (6) in AL-01 because grinding-induced flaws generated on the notch root do not exist in the simulation. In addition, the simulated results adopt the relation (6) even in porous materials. The simulated results represent an effective volume concept is applicable to porous ceramics. On the other hand, the applicability of effective volume is doubtful for experimental results, as mentioned in a previous section. The difference is caused by the sample size effect, as follows. Only 20 specimens were used in experiments although the strength data were calculated for 100 specimens in the simulation.

5 Conclusions

In this work, the influence of specimen geometry on the strength in porous alumina was investigated by experimental results, and discussed based on results in numerical simulation.

Materials were commercial alumina ceramics, which had different porosities of p = 0.803%, 34.9%, and 48.4%. Strength characteristics of smooth specimens of different size and of notched specimen for respective materials with different porosity were obtained under three-point bending. The average strength for each combination of material and specimen geometry was correlated with the effective volume. In specimens of dense alumina excepting notched specimens, the mean strength was well expressed by a unique relation with the effective volume independently of specimen geometry. It was revealed that the mean strength of notched specimens was lower than those of the other specimens, because of grinding defects around notch root. On the other hand, in porous materials, the mean strength depending on specimen geometry was not able to be correlated with the effective volume.

The pore distributions were quantified by binary-digitizing data in observation via a laser scanning microscope. Based on observed pore distribution, a fracture mechanics based simulation of Monte Carlo type was conducted by assuming that a pore is surrounded by a virtual crack and characteristics of crack distribution are the same as those of pore distribution in a material. The simulated results revealed that the effect of the specimen geometry on the strength was well explained by using a proposed simulation procedure.

References:

[1] Jones RL, Rowcliffe DJ, Tensile-strength distribution for silicon nitride and silicon carbide ceramics, *Ceramics Bulletin*, Vol.58, No.9, 1979, pp. 836-839.

[2] Shetty DK, Rosenfield AR, Bansal GK, Duckworth WH, Biaxial fracture studies of a glass-ceramic, *Journal of the American Ceramic Society*, Vol.64, No.1, 1981, pp. 1-4.

[3] Bansal GK, Duckworth WH, Niesz DE, Strength-size relations in ceramic materials: Investigation of an alumina ceramic, *Journal of the American Ceramic Society*, Vol.59, No.11-1, 1976, pp. 472-478.

[4] Katayama Y, Hattori Y, Effects of specimen size on strength of sintered silicon nitride, *Journal of the American Ceramic Society*, Vol.65, No.10, 1982, pp. C164-C165.

[5] Matsusue K, Takahara K, Hashimoto R, Strength evaluation test of hot-pressed silicon nitride at room temperature, *Yogyo-Kyokai-Shi*, Vol.90, No.1040, 1982, pp. 168-174.

[6] Matsusue K, Takahara K, Hashimoto R, Strength evaluation of pressureless-sintered SiC and reaction-sintered Si3N4 at room temperature, *Yogyo-Kyokai-Shi*, Vol.90, No.1041, 1982, pp. 280-282.

[7] Neal DM, Lenoe EM, Examination of size effects in the failure prediction of ceramic

material, *Fracture Mechanics of Ceramics*, Vol.5, 1983, pp. 387-401.

[8] Fessler H, Fricker DC, Godfrey DJ, A comparative study of the mechanical strength of reaction-bonded silicon nitride, *Ceramics for High-Performance Applications*, Vol.3, 1983, pp. 705-736.

[9] Shetty DK, Rosenfield AR, Duckworth WH, Statistical analysis of size and stress state effects on the strength of an alumina ceramic, *ASTM Special Technical Publication*, Vol.844, 1984, pp. 57-80.

[10] Yamada T, Hoshide T, Reliability of ceramic materials for static and cyclic loads, *Proceedings of ICOSSAR '85 II*, 1985, pp. 441-450.

[11] Soma T, Matsui M, Oda I, Tensile strength of a sintered silicon nitride, *Non-oxide Technical and Engineering Ceramics*, 1986, pp. 361-374.

[12] Kschinka BA, Perrella S, Nguyen H, Bradt RC, Strength of glass spheres in compression, *Journal of the American Ceramic Society*, Vol.69, No.6, 1986, pp. 467-472.

[13] Davis DGS, The statistical approach to engineering design in ceramics, *Proceedings of the British Ceramic Society*, Vol.22, 1973, pp. 429-452.

[14] Davidge RW. *Mechanical Behaviour of Ceramics*, Cambridge University Press, 1979, pp. 138.

[15] Miyazaki N, Hoshide T, Influence of porosity and pore-distributions on strength properties of porous alumina, *Journal of Materials Engineering and Performance*, Vol.27, No.8, 2018, pp. 4345-4354.

[16] Testing method for flexural strength (modulus of rupture) of fine ceramics at room temperature, JIS R 1601, *Japanese Industrial Standard*, Japanese Standards Association, 2008.

[17] Weibull W, A statistical theory of the strength of materials, In *Ingeniors Vetenskaps Akademiens Handlingar Nr 151*, Royal Swedish Institute for Engineering Research, Stockholm, 1939.

[18] Hoshide T, Hukui T, Yamada T, Effect of porosity on strength of zirconia refractory, *The Society of Materials Science, Japan*, Vol.37, No.421, 1988, pp. 1139-1145.

[19] Hoshide T, Masuda M, Dependence of strength on size of flaw dominating fracture in ceramics, *The Society of Materials Science, Japan*, Vol.44, No.501, 1995, pp. 108-113.

[20] Hoshide T, Inoue T, Simulation of anomalous behavior of a small flaw in strength of engineering ceramics, *Engineering Fracture Mechanics*, Vol.38, No.4-5, 1991, pp. 307-312.

[21] Hoshide T, Furuya H, Nagase Y, Yamada T, Fracture mechanics approach to evaluation of strength in sintered silicon nitride, *International Journal of Fracture*, Vol.26, No.3, 1984, pp. 229-239.

[22] Hoshide T, Grain fracture model and its application to strength evaluation in engineering ceramics, *Engineering Fracture Mechanics*, Vol.44, No.3, 1993, pp. 403-408.

[23] Murakami Y, Aoki A, Hasebe N, Itoh Y, Miyata H, Miyazaki N, et al, *Stress Intensity Factors Handbook Vol 1 & 2*, Pergamon Press, Oxford, 1987.

[24] Murakami Y, Hanson MT, Hasebe N, Itoh Y, Kishimoto K, Miyata H, et al, *Stress Intensity Factors Handbook Vol 3*, The Society of Materials Science, Japan, and Pergamon Press, Oxford, 1992.

[25] Murakami Y, Hasebe N, Itoh Y, Kishimoto K, Miyata H, Miyazaki N, et al, *Stress Intensity Factors Handbook Vol 4 & 5*, The Society of Materials Science, Japan, and Elsevier science, 2001.

[26] Hoshide T, Sugiyama H, Numerical analysis of sample-size effect on strength of alumina, *Journal of Materials Engineering and Performance*, Vol.22, No.1, 2013, pp. 1-8.